Contribution from the Department of Inorganic Chemistry, University of Newcastle upon Tyne, NE1 7RU, England

Crystal Structure of Bis(μ-bis(trifluoromethyl)phosphido)-hexacarbonyldiiron, $Fe_2(CO)_6[\mu\text{-}P(CF_3)_2]_2$

WILLIAM CLEGG

Received December 16, 1975 AIC50901A

Bis(μ-bis(trifluoromethyl)phosphido)-hexacarbonyldiiron crystallizes in the orthorhombic space group *Pnma*, with a = 20.261 (2), b = 12.591 (2), c = 7.422 (1) Å. The structure has been determined from 2167 x-ray counter intensities by Patterson and Fourier techniques and refined by full-matrix least-squares methods to R = 6.88% (5.09% weighted). There are four molecules in the unit cell, each lying across a crystallographic mirror plane passing through the bridging ligands. The large flap angle of the folded Fe_2P_2 ring (118.9°) and concomitant long Fe–Fe bond length (2.821 Å) are discussed in relation to the strong electron-withdrawing property of the CF_3 substituents on phosphorus.

Introduction

Phosphine and phosphido ligands are common in transition metal chemistry, and a great variety of alkyl and aryl substituents on the phosphorus atom have been used in syntheses and reported in structural studies. The trifluoromethyl substituent is of particular interest, because of the markedly different properties of trifluoromethylphosphine and -phosphido compounds and transition metal complexes compared with those of related compounds having other alkyl and aryl substituents on phosphorus.[1,2] The differences can normally be attributed to the strong electron-withdrawing effect of the CF_3 group.

Several dimeric complexes of transition metals have been prepared, with bridging bis(trifluoromethyl)phosphido ligands.[2,3] We have determined the crystal structure of one of these, the title compound, in order to compare the results with other bridged dimers and to assess the effects of the electron-withdrawing CF_3 groups on the bridging geometry.

Experimental Section

Crystal data: $[Fe(CO)_3P(CF_3)_2]_2$, mol wt 617.8, orthorhombic, a = 20.261 (2) Å, b = 12.591 (2) Å, c = 7.422 (1) Å, U = 1893.4 Å^3, d_{calcd} = 2.167 g cm^{-3}, d_{measd} = 2.16 g cm^{-3}, Z = 4, $F(000)$ = 1192, space group *Pnma*, Mo Kα radiation (Zr filtered), λ 0.710 69 Å, μ(Mo Kα) = 18.94 cm^{-1}.

Data Collection and Reduction. The red crystals were rectangular parallelepipeds. Preliminary precession photographs (Mo Kα radiation) gave initial values for the orthorhombic cell parameters. Systematic absences were as follows: $0kl$, $k + l$ odd; $hk0$, h odd. These indicate space group *Pnma* (No. 62) or $Pn2_1a$ (alternative orientation of $Pna2_1$, No. 33). The density was measured by flotation in 1,2-dibromoethane–bromobenzene.

A crystal showing six faces perpendicular to the unit cell edges and of dimensions ca. 0.2 × 0.2 × 0.4 mm (distances between pairs of opposite faces) was sealed in a thin-walled Lindemann glass capillary and mounted on a Hilger and Watts *Y*290 diffractometer, with the c axis (parallel to the longest measurement) misaligned about 15° from the spindle (ϕ) axis. The unit cell parameters and orientation matrix were obtained by a least-squares refinement[4] based on the setting angles of 12 reflections with 2θ between 40 and 55°, determined at room temperature by the *Y*290 automatic centering routines.

Intensities were collected at room temperature in the θ–2θ scan mode for $2\theta \leq 55°$.

All reflections with $h \geq 0$ and $k \geq 0$ were measured, giving two equivalent measurements for most reflections. Each reflection was scanned by 80 steps of 0.01° in θ, with a 2-s count at each step, and a 40-s background count at each end of the scanning range. Attenuators were inserted automatically for very intense reflections.

Three standard reflections were monitored after every 40 reflections, and their decay (about 2.5% by the end of the collection) was used to bring all the reflections to a common scale.

Intensities were calculated as $I = K(N - rB)$, where N and B are the integrated peak and total background counts, r is the ratio of total peak and backgound counting times, and K is a scale factor calculated from the standard reflection measurements and, where applicable, attenuator factors. Standard deviations were taken to be $\sigma(I) = K^2(N + r^2B) + I^2P^2$, with a value of 0.05 for the "instability factor" P. The usual Lorentz and polarization corrections were applied, but no absorption corrections.[5] Estimated transmission factors range from 0.68 to 0.71; the errors in the observed structure factors caused by neglect of absorption are thus less than 2%.

All reflections with positive recorded intensity were used in structure solution and refinement. The data were merged to give 2167 independent reflections. The agreement among equivalent reflections was measured by the index $R' = \{\sum w(F_1 - F_2)^2/\sum w\bar{F}^2\}^{1/2}$, the summations being over all pairs of equivalent reflections; $w = 1/\sigma^2(F)$. The value of R' was 3.3%.

The centrosymmetric space group *Pnma* was indicated by the statistical distribution of E values and was assumed in subsequent calculations.

Structure Solution and Refinement. The atoms were located from Patterson and Fourier syntheses, and parameters were refined by full-matrix least-squares methods. Atomic scattering factors for uncharged atoms, including corrections for anomalous scattering, were taken from ref 6. The molecule was found to lie across the mirror plane at $y = {}^1/_4$. The quantity minimized was $\sum w(F_o - F_c)^2$, with $w = 1/\sigma^2(F_o)$.

Three cycles of refinement with isotropic thermal parameters gave values for R ($=\sum|F_o - F_c|/\sum|F_o|$) and R_w ($=\{\sum w(F_o - F_c)^2/\sum wF_o^2\}^{1/2}$) of 14.2% and 14.3%, respectively. Anisotropic thermal parameters were introduced for all atoms, and several further cycles reduced R to 6.88% and R_w to 5.09%. The largest shift:esd ratio for the atomic coordinates in the last refinement cycle was 0.006 and, for the thermal parameters, 0.007. The final rms deviation of a reflection of unit weight on an absolute scale of F_c ($=\{\sum w(F_o - F_c)^2/\sum w\}^{1/2}$) was 1.45 electrons, and an analysis of this indicator as a function of indices, of sin θ, and of F_o showed no systematic trends, thus suggesting that the weighting scheme was consistent.[7] A comparison of F_o and F_c for strong low-angle reflections indicated no significant extinction effects; no correction was, therefore, made. A final difference synthesis showed no peaks larger than 0.8 e Å^{-3}, the largest being in the neighborhood of the fluorine atoms.

Bond lengths within two of the CF_3 groups were considerably shorter than those in the other two, and some of the thermal parameters of these fluorine atoms [F(51), F(52), F(61), F(62)] were very large. The thermal motion is depicted in Figure 1, for which the direction of view is chosen to show clearly the motion of these fluorine atoms. All four CF_3 groups show a considerable degree of torsional vibration about the P–C bonds, but for the two groups in question the amplitude of this vibration is very large. Three possible explanations were considered: (i) these figures do actually represent a large torsional oscillation of the two CF_3 groups concerned about the P–C bonds; such a motion results in a systematic reduction of bond lengths as measured by x-ray diffraction;[8] (ii) there is disorder of the CF_3 groups, the positions determined being the average for all of the actual locations of the atoms in the crystal structure and the high thermal parameters being the attempt by the refinement to cover the range of disorder as far as possible; (iii) the space group is actually $Pn2_1a$ with only an approximate mirror plane through the molecule.

Possibility (iii) was explored by applying small random shifts to the positional parameters for all the atoms in the molecule, in order to remove the mirror plane, and then refining in space group $Pn2_1a$

Table I. Atomic Coordinates ($\times 10^4$)[a] and Anisotropic Thermal Parameters ($Å^2 \times 10^4$)[a,b]

Atom	x	y	z	U_{11}	U_{22}	U_{33}	U_{23}	U_{13}	U_{12}
Fe	1282.3 (2)	1380.4 (4)	594.4 (7)	352 (3)	368 (3)	451 (3)	19 (2)	−17 (2)	11 (2)
P(1)	509 (1)	2500[c]	1414 (2)	341 (7)	427 (8)	400 (7)	0[c]	0 (6)	0[c]
P(2)	1935 (1)	2500	1995 (2)	336 (7)	470 (8)	467 (8)	0	−37 (6)	0
C(1)	770 (2)	860 (3)	−1210 (6)	549 (24)	422 (22)	596 (24)	10 (21)	−40 (20)	48 (19)
O(1)	478 (2)	489 (3)	−2335 (5)	1013 (26)	614 (21)	841 (23)	−187 (19)	−396 (21)	−20 (19)
C(2)	1166 (2)	329 (3)	2234 (6)	473 (24)	523 (24)	695 (28)	107 (23)	−110 (21)	−31 (19)
O(2)	1089 (2)	−302 (3)	3273 (5)	865 (25)	769 (23)	959 (27)	448 (22)	−133 (20)	−132 (19)
C(3)	1973 (2)	804 (3)	−612 (6)	517 (23)	496 (24)	662 (26)	−89 (22)	−9 (22)	44 (20)
O(3)	2376 (2)	388 (3)	−1376 (5)	663 (22)	874 (25)	1188 (30)	−377 (23)	149 (20)	212 (19)
C(4)	−301 (3)	2500	128 (9)	351 (28)	510 (35)	716 (41)	0	−6 (28)	0
F(41)	−191 (2)	2500	−1630 (5)	543 (20)	920 (28)	558 (23)	0	−121 (17)	0
F(42)	−668 (1)	1654 (2)	495 (4)	541 (14)	756 (18)	979 (21)	108 (17)	−93 (14)	−225 (13)
C(5)	141 (3)	2500	3717 (9)	471 (34)	720 (43)	526 (34)	0	48 (30)	0
F(51)	577 (2)	2500	4949 (6)	833 (32)	2815 (78)	486 (23)	0	61 (24)	0
F(52)	−219 (3)	1697 (4)	4067 (5)	2436 (51)	1887 (39)	964 (27)	−424 (27)	925 (32)	−1415 (39)
C(6)	2072 (4)	2500	4506 (10)	687 (45)	1009 (60)	514 (38)	0	−145 (37)	0
F(61)	2685 (3)	2500	4972 (7)	788 (34)	4017 (120)	761 (33)	0	−404 (28)	0
F(62)	1810 (2)	1666 (3)	5300 (4)	1802 (37)	1042 (25)	578 (19)	204 (18)	−77 (21)	−91 (25)
C(7)	2842 (3)	2500	1311 (10)	320 (30)	628 (41)	842 (47)	0	−53 (31)	0
F(71)	2893 (2)	2500	−457 (6)	503 (21)	831 (27)	850 (29)	0	198 (20)	0
F(72)	3157 (1)	1646 (2)	1921 (5)	454 (14)	875 (20)	1337 (27)	235 (20)	−104 (16)	158 (14)

[a] In this and subsequent tables, estimated standard deviations in the last place of figures are given in parentheses. [b] The anisotropic temperature factor takes the form $\exp[-2\pi^2(h^2a^{*2}U_{11} + \ldots + 2hka^*b^*U_{12} + \ldots)]$. [c] Parameters without esd's are fixed by space group symmetry.

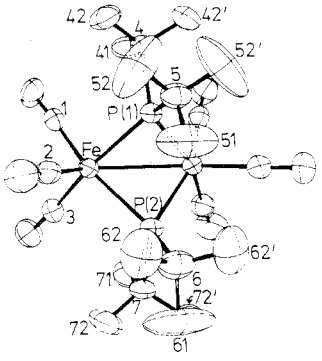

Figure 1. Perspective view showing thermal motion as 40% probability contours. For clarity, carbon and fluorine atoms are labeled by number only (the prime indicates an atom reflected across the mirror plane passing through the bridging ligands), and obscured ellipsoids and bonds are shown dotted.

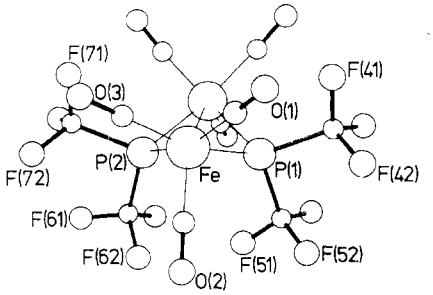

Figure 2. Perspective view of the $Fe_2(CO)_6[\mu\text{-}P(CF_3)_2]_2$ molecule, showing the folded Fe_2X_2 ring typical of $Fe_2(CO)_6[\mu\text{-}X]_2$ compounds. The numbering of the carbon atoms [C(1)–C(7)] follows that of the oxygen and fluorine atoms; labels are omitted for clarity.

with a damping factor applied to the refinement to reduce matrix singularity problems and one y coordinate fixed to define the unit cell origin. The parameters refined back toward the *Pnma* values.

Simple disorder models were tested, with partially occupied sites for fluorine atoms, but in all cases thermal parameters remained high, no significant reduction in R_w or R was observed, and bond length constraints were necessary with sites of low partial occupancy.

Possibilities (ii) and (iii) were, therefore, rejected as being either incorrect or unworkable, and the high thermal parameters were accepted as real.

Observed and calculated structure factors on an absolute scale (electrons) are tabulated as supplementary material. Positional and thermal parameters are given in Table I, interatomic distances and bond angles in Table II, and selected planes through atomic positions in Table III. The full covariance matrix was used in estimating standard deviations in distances and angles.

Results

The molecular structure is shown in Figure 2, with a direction of view which emphasizes the central folded Fe_2P_2 ring. The molecule has crystallographic m (C_s) symmetry, and approximate $mm2$ (C_{2v}) symmetry if the orientation of the CF_3 groups is ignored. The crystallographic mirror plane passes through the bridging phosphido groups. The basic geometry of the central Fe_2P_2 ring is typical of $Fe_2(CO)_6(\mu\text{-}X)_2$ compounds:[9-19] the ring can be thought of as folded about the Fe–Fe bond, with a flap angle of 120.6°, or about the P···P line, with a flap angle of 118.9°.

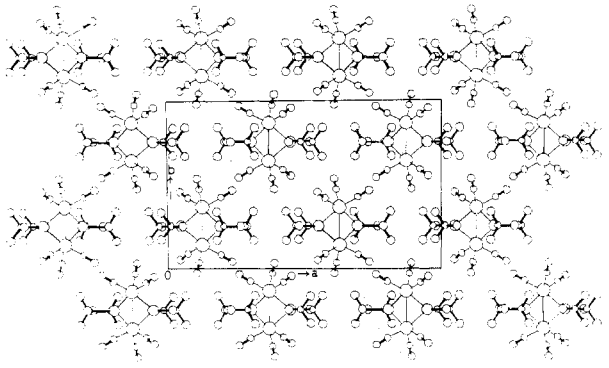

Figure 3. Projection along the z axis.

Table IV compares some important features of the structure with corresponding results for other $Fe_2(CO)_6(\mu\text{-}PRR')_2$ compounds.[19] The significant differences between the present compound and the others are (i) a much longer Fe–Fe bond, (ii) a shorter Fe–P bond, (iii) a larger Fe–P–Fe angle, and (iv) a much larger flap angle. These features are, of course, all interrelated and are discussed below.

Fe–C and C–O bond lengths are typical of the values observed in iron carbonyl complexes. The metal–carbonyl groups are all essentially linear.

The crystal packing is shown in Figure 3, by a projection of the structure along the crystallographic z axis. There are no unusual intermolecular interactions (see Table II).

Table II

Bond Lengths, Å

Fe-P(1)	2.193 (1)	P(2)-C(6)	1.884 (7)
Fe-P(2)	2.194 (1)	P(2)-C(7)	1.907 (6)
Fe-Fe'[a]	2.819 (1)	C(4)-F(41)	1.324 (7)
Fe-C(1)	1.817 (4)	C(4)-F(42)	1.328 (4)
Fe-C(2)	1.813 (4)	C(5)-F(51)	1.271 (7)
Fe-C(3)	1.812 (4)	C(5)-F(52)	1.273 (5)
C(1)-O(1)	1.125 (5)	C(6)-F(61)	1.291 (8)
C(2)-O(2)	1.118 (5)	C(6)-F(62)	1.315 (5)
C(3)-O(3)	1.125 (5)	C(7)-F(71)	1.316 (8)
P(1)-C(4)	1.900 (6)	C(7)-F(72)	1.330 (4)
P(1)-C(5)	1.865 (6)		

Bond Angles, Deg

Fe'-Fe-P(1)	50.0 (1)	C(4)-P(1)-C(5)	96.6 (3)
Fe'-Fe-P(2)	50.0 (1)	Fe-P(2)-Fe'	79.9 (1)
Fe'-Fe-C(1)	111.2 (1)	Fe-P(2)-C(6)	123.8 (2)
Fe'-Fe-C(2)	136.9 (1)	Fe-P(2)-C(7)	117.1 (2)
Fe'-Fe-C(3)	113.6 (1)	C(6)-P(2)-C(7)	97.0 (3)
P(1)-Fe-P(2)	83.5 (1)	P(1)-C(4)-F(41)	110.5 (4)
P(1)-Fe-C(1)	91.6 (1)	P(1)-C(4)-F(42)	112.4 (3)
P(1)-Fe-C(2)	101.0 (1)	F(41)-C(4)-F(42)	107.3 (4)
P(1)-Fe-C(3)	161.0 (1)	F(42)'-C(4)-F(42)	106.8 (5)
P(2)-Fe-C(1)	157.7 (1)	P(1)-C(5)-F(51)	112.4 (4)
P(2)-Fe-C(2)	103.3 (1)	P(1)-C(5)-F(52)	114.6 (4)
P(2)-Fe-C(3)	91.5 (1)	F(51)-C(5)-F(52)	104.5 (5)
C(1)-Fe-C(2)	99.0 (2)	F(52)'-C(5)-F(52)	105.1 (7)
C(1)-Fe-C(3)	86.1 (2)	P(2)-C(6)-F(61)	114.0 (6)
C(2)-Fe-C(3)	98.0 (2)	P(2)-C(6)-F(62)	112.6 (3)
Fe-C(1)-O(1)	175.9 (4)	F(61)-C(6)-F(62)	105.6 (4)
Fe-C(2)-O(2)	178.4 (4)	F(62)'-C(6)-F(62)	105.9 (6)
Fe-C(3)-O(3)	175.4 (4)	P(2)-C(7)-F(71)	109.9 (4)
Fe-P(1)-Fe'	80.0 (1)	P(2)-C(7)-F(72)	111.8 (3)
Fe-P(1)-C(4)	118.6 (1)	F(71)-C(7)-F(72)	107.6 (4)
Fe-P(1)-C(5)	122.7 (1)	F(72)'-C(7)-F(72)	108.0 (5)

Shortest Intermolecular Distances of Various Types

Type	Atoms	Dist, Å	Transformation[b]
O···O	O(3)···O(2)	3.122	$^1/_2 - x, -y, ^1/_2 + z$
	O(2)···O(1)	3.258	$-x, -y, -z$
F···O	F(42)···O(1)	3.048	$-x, -y, -z$
	F(72)···O(3)	3.053	$^1/_2 - x, -y, -^1/_2 + z$
	F(52)···O(1)	3.083	$-x, -y, -z$
	F(62)···O(3)	3.161	$x, y, -1 + z$
	F(52)···O(2)	3.177	$-x, -y, 1 - z$
	F(51)···O(1)	3.243	$x, y, -1 + z$
	F(62)···O(3)	3.310	$^1/_2 - x, -y, -^1/_2 + z$
F···F	F(51)···F(41)	2.978	$x, y, -1 + z$
	F(72)···F(42)	3.057	$-^1/_2 + x, y, ^1/_2 - z$

[a] The prime indicates an atom reflected across the mirror plane at $y = ^1/_4$. [b] The distances given are between the second atom in one molecule and the first atom in another molecule related by the symmetry transformations shown.

Table III. Equations of Planes through Atomic Positions, Referred to an Angstrom Coordinate System on the Crystal Axes

Plane	Atoms	Equation
1	Fe, P(1), P(2)	$-0.1271X - 0.5086Y + 0.8516Z = -0.8385$
2	Fe', P(1), P(2)	$-0.1271X + 0.5086Y + 0.8516Z = 2.3632$
3	Fe, Fe', P(1)	$0.3619X + 0.9322Z = 1.3516$
4	Fe, Fe', P(2)	$-0.6179X + 0.7862Z = -1.2586$

Planes	Dihedral angle, deg	Planes	Dihedral angle, deg
1-2	118.9	3-4	120.6

Discussion

Some 20 structures of the type $Fe_2(CO)_6(\mu\text{-}X)_2$ are now known,[19] with a variety of bridging ligands. The "effective atomic number" rule and the observed diamagnetism require the postulation of an iron–iron interaction equivalent to a single bond, and the basic structure is commonly regarded as being made up of two tetragonal-pyramidal $Fe(CO)_3X_2$ units joined along the X···X basal edge, with a bent iron–iron bond controlling the folding of the central Fe_2X_2 ring about this edge.[9,16] The existence and bent nature of the iron–iron interaction has been demonstrated from nonparametrized molecular orbital calculations.[20]

The detailed geometry of the central Fe_2X_2 ring varies considerably with the bridging ligand X but different substitutuents on the bridging atom produce much smaller differences than changing the bridging atom itself. Thus, nitrogen-bridged compounds[9-15,19] have Fe–Fe distances in the range 2.37–2.416 Å, Fe–N distances of 1.94–2.02 Å, Fe–N–Fe angles of 72.5–75.0°, and flap angles of 88–103.6°; for sulfur-bridged compounds[16-19] the ranges are Fe–Fe = 2.507–2.540 Å, Fe–S = 2.248–2.274 Å, Fe–S–Fe = 67.3–68.8°, and flap angles of 87.9–95.2°; for phosphorus-bridged compounds[19] (excluding the title compound), they are Fe–Fe = 2.619–2.665 Å, Fe–P = 2.203–2.233 Å, Fe–P–Fe = 72.0–74.3°, and flap angles of 100–107.3° (see Table IV). The present structure stands out in Table IV as having features well outside the range for the other phosphorus-bridged compounds.

This marked difference is unlikely to be due to purely steric effects; the various groups attached to phosphorus in the other complexes in Table IV (H, CH_3, C_6H_5) are quite different in size and shape, yet the variation in the geometry of the central ring is small compared with the changes on replacing these groups by CF_3. Moreover, the planar Fe_2P_2 ring in $Fe_2(NO)_4[\mu\text{-}P(CF_3)_2]_2$ has a Fe–Fe distance of 2.747 (1) Å,[21] over 0.2 Å longer than the Ni–Ni distances of 2.505 (1) and 2.515 (2) Å in the two crystallographically independent molecules of the isoelectronic $Ni_2(CO)_4[\mu\text{-}PPh_2]_2$,[22] and the steric crowding of the CF_3 groups in this molecule will be rather less than that in the present complex, because the flattening of the central ring pulls the two bridging ligands further apart. Nor can crystal packing be the main cause, for $Fe_2(NO)_4[\mu\text{-}P(CF_3)_2]_2$ crystallizes in the triclinic space group $P\bar{1}$, with a completely different packing arrangement.

A simple rationalization can be found in isovalent hybridization arguments,[23] as follows.[24,25] Consider the Fe_2PX_2 fragment (**1**). As the electronegativity of X is increased, so

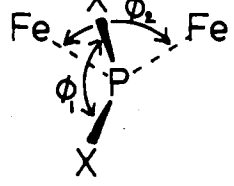

1

the phosphorus orbitals used for P–X bond formation will have greater p character; this produces a smaller X–P–X angle ϕ_1 (ca. 13° below the normal tetrahedral angle when X = CF_3). Consequently, more phosphorus s character is left for bonding to the iron atoms, and the result is a larger Fe–P–Fe angle ϕ_2. The longer Fe–Fe bond length and larger flap angle necessarily follow. The larger phosphorus s character also means that the Fe–P bonds should be shorter when X is CF_3, and this is indeed the case (but the situation is complicated by the question of the π-bonding contribution). Although this simple argument gives a rationalization of the variation in these structural features, it must be regarded with some caution, because s–p hybridization can only really be discussed with reference to bond angles between 90° (pure p) and 180° (sp hybrids), without introducing "bent bonds".

Extended Hückel-type molecular orbital calculations have been made on the $Fe_2(CO)_6(\mu\text{-}X)_2$ system.[25,26] The results

Table IV. Features of $Fe_2(CO)_6(\mu\text{-}PRR')_2$ Complexes[a]

R, R'	Fe–Fe	Fe–P	P...P	Fe–P–Fe	P–Fe–P	Flap angle[b]
C_6H_5, C_6H_5	2.623 (3)	2.233 (3)	2.866 (3)	72.0 (1)	79.9 (1)	100.0
C_6H_5, CH_3	2.619 (1)	2.217 (1)	2.864 (2)	72.4 (1)	80.5 (1)	101.4
C_6H_5, H	2.662 (1)	2.212 (1)	2.790 (2)	74.0 (1)	78.2 (1)	101.7
CH_3, H	2.661 (1)	2.203 (1)	2.725 (2)	74.3 (1)	76.4 (1)	100.5
CH_3, CH_3	2.665 (2)	2.209 (2)	2.925 (4)	74.2 (1)	82.9 (1)	107.3
CF_3, CF_3	2.819 (1)	2.193 (1)	2.921 (2)	80.0 (1)	83.5 (1)	118.9

[a] Distances in angstroms; angles in degrees; data for all but the title compound are taken from a table in ref 19. [b] This is the flap angle for folding of the Fe_2P_2 ring about the P···P line, i.e., the angle between the two FeP_2 planes.

are qualitatively similar to the simple argument above, and good agreement is obtained between the main features of the observed structures and the calculations. A brief summary of Burdett's treatment[25] is given here, pending publication of the details. The model compound for the calculations was $Fe_2(CO)_6(\mu\text{-}PF_2)_2$, with molecular geometry idealized to C_{2v} symmetry from the observed structure of $Fe_2(CO)_6[\mu\text{-}P(CF_3)_2]_2$; the CF_3 groups were replaced by fluorine atoms for purposes of simplifying the calculations. The valence molecular orbitals were constructed, and their energies and make-up from atomic orbitals were studied as functions of (i) the flap angle and (ii) the electronegativity of the "fluorine" atoms (by varying orbital parameters for these atoms) and the F–P–F angle. This is a different approach from that of Dahl and co-workers,[20] who looked at the nature of the molecular orbitals for fixed geometries with the aim of elucidating the character and direction of Fe–Fe bonding.

The main feature emerging was that the iron–phosphorus bonding interactions were much greater than the iron–iron interactions; in terms of bond overlap populations, that between iron and phosphorus is between one and two orders of magnitude larger than that between the metal atoms. Second, the energy of the highest occupied molecular orbital (HOMO) is found to vary with flap angle rather more than the lower energy occupied orbitals, so it is the nature of this orbital which will largely determine the observed flap angle. The main iron and phosphorus atomic orbital contributions to the a_1 HOMO are represented in **2**: a combination of metal d_{z^2} and d_{yz} and

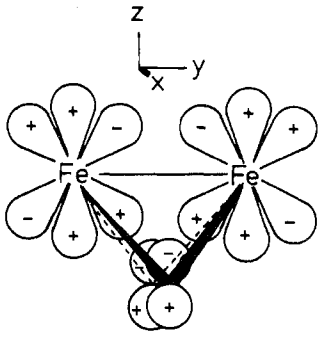

2

phosphorus p_y. The HOMO is thus iron–iron bonding and iron–phosphorus antibonding, and the equilibrium values of the flap angle and Fe–Fe distance are governed by the balance of these two effects. Increasing the flap angle (and hence the Fe–Fe distance) weakens the Fe–Fe interaction but also decreases Fe–P repulsions. (It is interesting to note in passing that the maximum electron density between the iron atoms in the HOMO will not lie on the direct Fe–Fe line, but above it, because of the Fe–P antibonding contribution; this corresponds nicely to the "bent bond" description.) Third, the HOMO is P–X antibonding, so the more electronegative X is, the greater is the contribution of phosphorus p_y to the HOMO and the smaller is the contribution of X atomic orbitals. (This is supported experimentally by ESR spectra of BX_2 radicals in inert-gas matrices, with B = N, P; X = F, Cl.[27] The reverse reasoning would apply if the HOMO were P–X bonding.) This leads to greater Fe–P antibonding interactions and, therefore, a larger flap angle.

Conclusion

The observed molecular structure of bis(μ-bis(trifluoromethyl)phosphido)-hexacarbonyldiiron clearly demonstrates the effect of the strongly electron-withdrawing CF_3 substituents on the geometry of the central Fe_2P_2 ring. The substituents, vis a vis alkyl and aryl groups, cause a widening of the Fe–P–Fe angle and hence a larger flap angle and longer metal–metal bond. In bridged dimers of this type, "electron counting" requires a formal metal–metal bond, but the length and strength of this bond seem to be secondary to the electronic effects of the bridging ligands and the metal–bridge bonding.

Acknowledgment. The author thanks Dr. R. C. Dobbie for providing crystals and Dr. H. M. M. Shearer for assistance in the data collection at Durham University. Calculations were performed on the IBM370/165 computer at Cambridge University and the IBM370/168 and Hewlett-Packard 2000E computers at Newcastle University. Gratitude is expressed to Professor L. F. Dahl for prepublication data and to Dr. J. K. Burdett for his interest and many helpful discussions.

Registry No. $Fe_2(CO)_6[\mu\text{-}P(CF_3)_2]_2$, 21729-52-2.

Supplementary Material Available: Listing of structure factor amplitudes (13 pages). Ordering information is given on any current masthead page.

References and Notes

(1) A. B. Burg, *Acc. Chem. Res.*, **2**, 353 (1969).
(2) R. C. Dobbie, M. J. Hopkinson, and D. Whittaker, *J. Chem. Soc., Dalton Trans.*, 1030 (1972).
(3) J. Grobe, *Z. Anorg. Allg. Chem.*, **331**, 63 (1964); **361**, 32, 47 (1968); J. Grobe and H. Stierand, *ibid.*, **371**, 99 (1969).
(4) W. R. Busing and H. A. Levy, *Acta Crystallogr.*, **22**, 457 (1967).
(5) Computer programs used in this study, other than those of the author, were local versions of the following: for crystal structure determination and refinement, SHEL-X (G. M. Sheldrick, Cambridge, England); for geometrical calculations on final atomic positions, XANADU (G. M. Sheldrick and P. J. Roberts, Cambridge); for Figure 1, ORTEP (C. K. Johnson, Oak Ridge, Tenn.); for Figures 2 and 3, PLUTO (W. D. S. Motherwell, Cambridge).
(6) D. T. Cromer and J. T. Waber, "International Tables for X-Ray Crystallography", Vol. IV, Kynoch Press, Birmingham, England, 1974, p 99; D. T. Cromer and J. A. Ibers, *ibid.*, p 149.
(7) W. C. Hamilton, ref 6, p 293.
(8) D. W. J. Cruickshank, *Acta Crystallogr.*, **9**, 757 (1956); **14**, 896 (1961).
(9) $Fe_2(CO)_6[\mu\text{-}NH_2]_2$: L. F. Dahl, W. R. Costello, and R. B. King, *J. Am. Chem. Soc.*, **90**, 5422 (1968).
(10) $Fe_2(CO)_6[(\mu\text{-}NCH_3)_2CO]$: R. J. Doedens, *Inorg. Chem.*, **7**, 2323 (1968).
(11) $Fe_2(CO)_6[(\mu\text{-}NC_6H_5)_2CO]$: J. A. J. Jarvis, B. E. Job, B. T. Kilbourn, R. H. B. Mais, P. G. Owston, and P. F. Todd, *Chem. Commun.*, 1149 (1967).
(12) $Fe_2(CO)_6[(\mu\text{-}NH)C_6H_4(\mu\text{-}NC_6H_5)]$: P. E. Baikie and O. S. Mills, *Inorg. Chim. Acta*, **1**, 55 (1967).
(13) $Fe_2(CO)_6[\mu\text{-}NHN{=}C(p\text{-}C_6H_4CH_3)_2]_2$: M. M. Bagga, P. E. Baikie, O. S. Mills, and P. L. Pauson, *Chem. Commun.*, 1106 (1967).
(14) $Fe_2(CO)_6[(\mu\text{-}NH)_2C_6H_4]$: P. E. Baikie and O. S. Mills, *Chem. Commun.*, 707 (1966).
(15) $Fe_2(CO)_6[\mu\text{-}N{=}C(p\text{-}C_6H_4CH_3)_2]_2$: D. Bright and O. S. Mills, *Chem. Commun.*, 245 (1967).
(16) $Fe_2(CO)_6[\mu\text{-}SC_2H_5]_2$: L. F. Dahl and C.-H. Wei, *Inorg. Chem.*, **2**, 328 (1963).
(17) $Fe_2(CO)_6[(\mu\text{-}S)_2C_2(C_6H_5)_2]$: H. P. Weber and R. F. Bryan, *J. Chem. Soc. A*, 182 (1967).
(18) $[Fe_2(CO)_6(\mu\text{-}SCH_3)]_2(\mu_4\text{-}S)$: J. M. Coleman, A. Wojcicki, P. J. Pollick, and L. F. Dahl, *Inorg. Chem.*, **6**, 1236 (1967).

(19) J. R. Huntsman and L. F. Dahl, to be submitted for publication.
(20) B. K. Teo, M. B. Hall, R. F. Fenske, and L. F. Dahl, *Inorg. Chem.*, **14**, 3103 (1975).
(21) W. Clegg, work in preparation.
(22) J. A. Jarvis, R. H. B. Mais, P. G. Owston, and D. T. Thompson, *J. Chem. Soc. A*, 1867 (1970).
(23) R. S. Mulliken, *J. Phys. Chem.*, **41**, 318 (1937); **56**, 295 (1952); H. A. Bent, *J. Chem. Phys.*, **33**, 1259 (1960).
(24) L. F. Dahl, personal communication.
(25) J. K. Burdett, to be submitted for publication.
(26) R. H. Summerville and R. Hoffmann, to be submitted for publication.
(27) M. S. Wei, J. H. Current, and J. Gendell, *J. Chem. Phys.*, **57**, 2431 (1972).

Contribution from the Departments of Chemistry, Colorado State University, Fort Collins, Colorado 80523, and Western Washington State College, Bellingham, Washington 98225

Crystal and Molecular Structure of Cyano(2,2′,2″-terpyridine)copper(II) Nitrate Monohydrate

OREN P. ANDERSON,*[1a] ALAN B. PACKARD,[1a] and MARK WICHOLAS[1b]

Received December 23, 1975 AIC50915G

The crystal and molecular structure of cyano(2,2′,2″-terpyridine)copper(II) nitrate monohydrate, $[Cu(N_3C_{15}H_{11})CN](NO_3)\cdot H_2O$, has been determined from three-dimensional single-crystal x-ray diffraction data, collected by counter techniques. The blue-green crystals are monoclinic, space group $P2_1/c$ (No. 14), with four formula units in a unit cell of dimensions $a = 12.230$ (11) Å, $b = 7.742$ (6) Å, $c = 17.160$ (15) Å, and $\beta = 90.93$ (5)°. The structure was refined by full-matrix least-squares methods to an R of 0.069 ($R_w = 0.073$) for 1124 independent reflections with $F^2 > 3\sigma(F^2)$. The coordination geometry about the copper(II) ion is based on a distorted square pyramid. Three of the basal coordination positions are occupied by nitrogen atoms of the terpyridine ligand (Cu–N = 1.94 (1), 2.05 (1), 2.06 (1) Å), with the fourth position occupied by cyanide ion (Cu–C = 1.92 (2) Å). The copper(II) ion is displaced 0.26 Å out of the basal plane of four coordinating atoms, toward the nitrogen end (Cu–N = 2.21 (1) Å) of a cyanide bonded to a symmetry-related copper(II) ion. This extended interaction involving nonlinear (Cu–N–C = 164 (1)°) cyanide bridges between copper ions extends through the lattice along the crystallographic twofold screw axis.

Introduction

We have previously discussed[2] the intriguing aspects of the coordination chemistry of copper(II). Specifically, these include the variety of coordination geometries possible about copper(II), the subtle asymmetries induced in these geometries by the $3d^9$ electronic distribution, and the relative stabilities of the cupric and cuprous oxidation states.

The cyanide ion, which normally reduces the copper(II) ion to cuprous cyanide,[3] has been shown to engage in stable binding to the cupric ion, provided that the copper(II) is first protected against reduction by coordination of stabilizing ligands which prefer to bind to the metal in the dipositive oxidation state.[4,5] The structures of three complexes in which the cyanide ion is bonded directly to the cupric ion have been fully reported.[2,6,8] In the monomeric cyanobis(1,10-phenanthroline)copper(II) nitrate monohydrate,[2] the overall coordination geometry about copper(II) was found to be trigonal bipyramidal, with the cyanide ion occupying one of the equatorial sites. In that structure, the nitrogen end of the cyanide ligand was involved in hydrogen-bonding to the lattice water of hydration. In the dimeric complex $[Cu_2A_2(CN)](ClO_4)_3$ (A = 5,7,7,12,14,14-hexamethyl-1,4,8,11-tetraazacyclotetradeca-4,11-diene), cyanide was observed[6] to occupy an equatorial position in a trigonal-bipyramidal coordination geometry about each copper and to bridge the two cupric ions directly in a linear fashion. This bridging mode is generally accepted as normal for the cyanide ion, although other modes of bridging have occasionally been demonstrated.[7] Finally, in the complex $[Cu_2(tren)_2(CN)_2](BPh_4)_2$ (tren = 2,2′,2″-triaminotriethylamine), each complex ion again exhibited trigonal-bipyramidal stereochemistry, with cyanide found to occupy an axial position in this case. The dimeric interaction in this last compound involved hydrogen bonds between the cyanide nitrogen and a hydrogen atom on a coordinated primary amine nitrogen of a second complex ion.[8]

As part of our continuing studies on the mode of binding of the cyanide ion to copper(II), we have synthesized the compound cyano(2,2′,2″-terpyridine)copper(II) nitrate monohydrate. The most obvious possible coordination geometry for this complex, considering the known geometry of the terdentate 2,2′,2″-terpyridine ligand (hereafter abbreviated as terpy), would involve square-planar coordination of the copper(II) ion, with bonding from the copper ion to the three nitrogen atoms of the terpy ligand and to the carbon atom of the cyano group. In view of the clear propensity already established for five-coordination at copper(II) when cyanide is involved in the bonding to the metal (vide supra) and in view of the well-established tendency of copper(II) to engage in the "4 + 1" mode of bonding,[9] it was considered to be quite possible that this complex might exhibit a five-coordinate, square-pyramidal structure, with water, or perhaps nitrate ion, occupying the out-of-plane coordination site at a long distance[10] from the copper(II) ion. Either of these possibilities would represent a new mode of participation for the cyanide ion in the copper(II) coordination sphere.

To ascertain the mode of bonding of the cyanide ion and the overall coordination geometry in this novel complex, an x-ray crystallographic study was undertaken on the title compound, cyano(2,2′,2″-terpyridine)copper(II) nitrate monohydrate.

Experimental Section

Synthesis of $[Cu(terpy)CN](NO_3)\cdot H_2O$. A 0.25-g ($1.07 \times 10^{-3}$ mol) portion of 2,2′,2″-terpyridine (terpy, purchased from G. F. Smith Chemical Co., Inc.) was dissolved in a 25-ml aqueous solution containing 0.24 g (1.05×10^{-3} mol) of $Cu(NO_3)_2\cdot 3H_2O$. Heating and stirring dissolved the terpy, with subsequent formation of a Cu^{II}–terpy complex. A 10-ml aqueous solution containing 0.070 g (1.07×10^{-3} mol) of KCN was added dropwise (with stirring) to the warm solution of the Cu^{II}–terpy complex. After filtration of the mixture while warm, the blue filtrate was allowed to cool slowly to room temperature. The resulting bluish green crystals were filtered, washed with distilled water, and dried over P_2O_5 for 24 h. The yield was 0.21 g (50%).

Characterization of $[Cu(terpy)CN](NO_3)\cdot H_2O$. Analysis was performed by Galbraith Laboratories, Knoxville, Tenn. Anal. Calcd